Supplementary Information

Elastomeric Microwell-Based Triboelectric Nanogenerators by in situ Simultaneous Transfer-Printing

Injamamul Arief,[a*] Philipp Zimmermann,[a] Sakrit Hait,[a] Hyeyoung Park,[a] Anik Kumar Ghosh,[a] Andreas Janke,[a] Santanu Chattopadhyay,[b] Jürgen Nagel,[a] Gert Heinrich,[c] Sven Wießner,[ad] Amit Das[a]

[a] *Leibniz-Institut für Polymerforschung Dresden e. V., Hohe Straße 6, D-01069 Dresden, Germany*

[b] *Rubber Technology Centre, Indian Institute of Technology Kharagpur, 721302, India*
[c] *Technische Universität Dresden, Institut für Textilmaschinen und Textile Hochleistungswerkstofftechnik, Hohe Straße 6, D-01069 Dresden, Germany*
[d] *Technische Universität Dresden, Institut für Werkstoffwissenschaft, Helmholtzstraße 7a, D-01069 Dresden, Germany*

*Corresponding author: I. Arief (E-mail: arief@ipfdd.de)

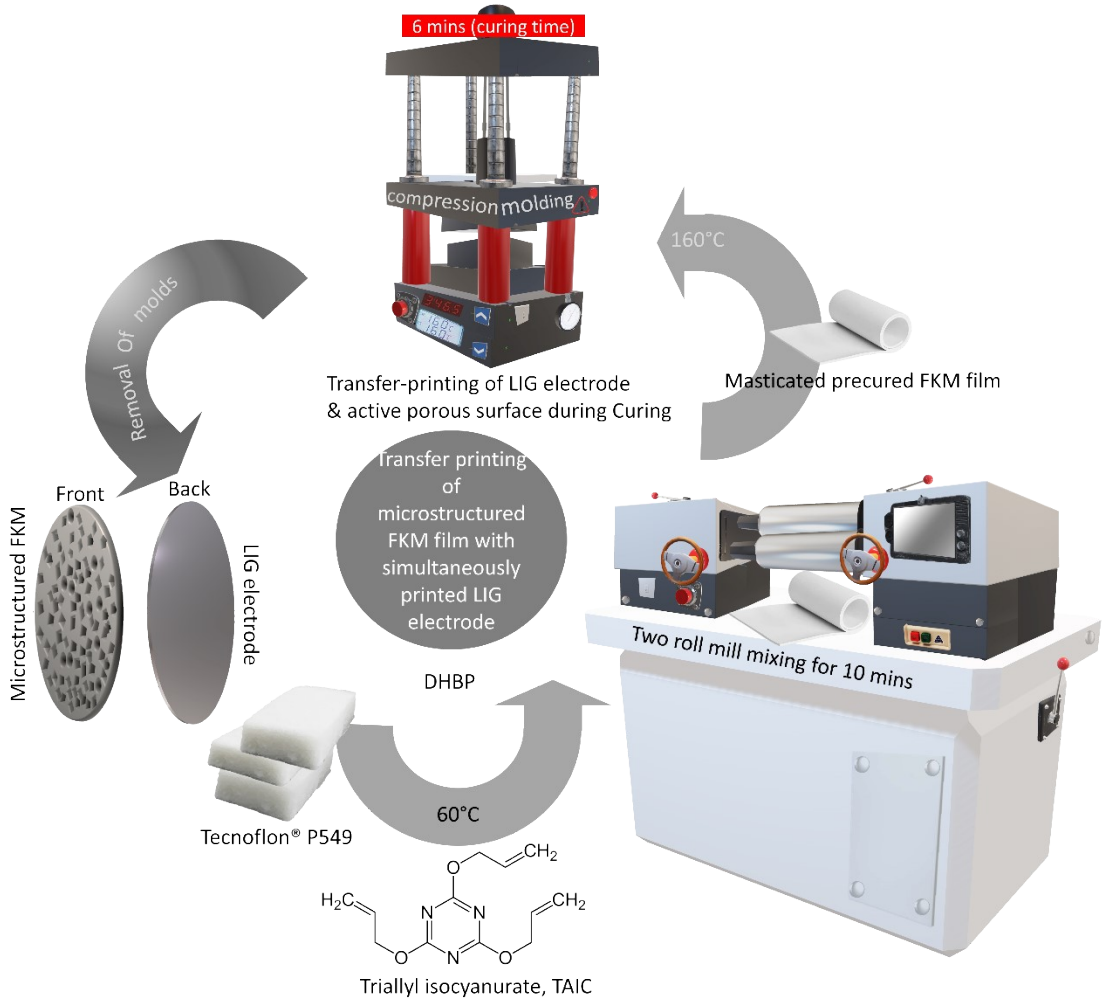

Figure S1. Schematic illustration of the fabrication process involving FKM elastomer processing and simultaneous curing-cum-stamping of the active surface and LIG electrode.

FKM (Fluororubber, Tecnoflon P549 L with Mooney viscosity ML_{1+10} ~24 at 120°C, fluorine content ~ 70 %) was first masticated for 1 min in a laboratory scale two-roll mill (Polymix 110L, size: 203×102 mm^2, Servitech GmbH, Wustermark, Germany) at 60 °C with a friction ratio of 1:1.2. Then 2,5-Dimethyl-2,5-di-(tert-butylperoxy)hexane (DBPH) and triallyl isocyanurate (TAIC) were added and mixed properly for 10 minutes.

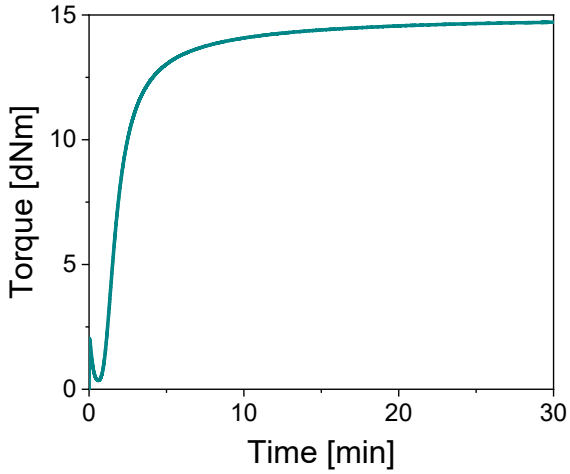

Figure S2. Rheometric torque profile from movie die rheometer. To study the rheometric characteristics, a specific amount (~5 g) of mixed FKM compound was subjected to moving die rheometer (Scarabaeus SIS-V50) for 1 hour at 160 °C with a frequency of 10 Hz. From rheometric torque-time profile, various parameters obtained are summarized in Table S1. Here t_2 represents the scorch time and scorch implies premature vulcanization. In this case the compound is less resistant towards scorch as the value is too small. t_{90} indicates the optimum cure time, i.e., time to attain 90% curing of the compound. M_H and M_L represent the maximum and minimum torque value of the compound. $(M_H - M_L)$ is defined as the extent of vulcanization, which corresponds to the state of crosslinking. Evidently, a higher value indicates a higher extent of crosslinking. Cure rate index (CRI) was calculated using the following equation:

$$CRI = \frac{100}{t_{90} - t_2}$$

Table S1. Parameters obtained from moving die rheometer

Parameters	Obtained value
t_2 (min)	0.84
t_{90} (min)	5.59
M_H (dN.m)	14.71
M_L (dN.m)	0.35
$M_H - M_L$ (dN.m)	14.36
Cure rate index (CRI) (min^{-1})	21.05

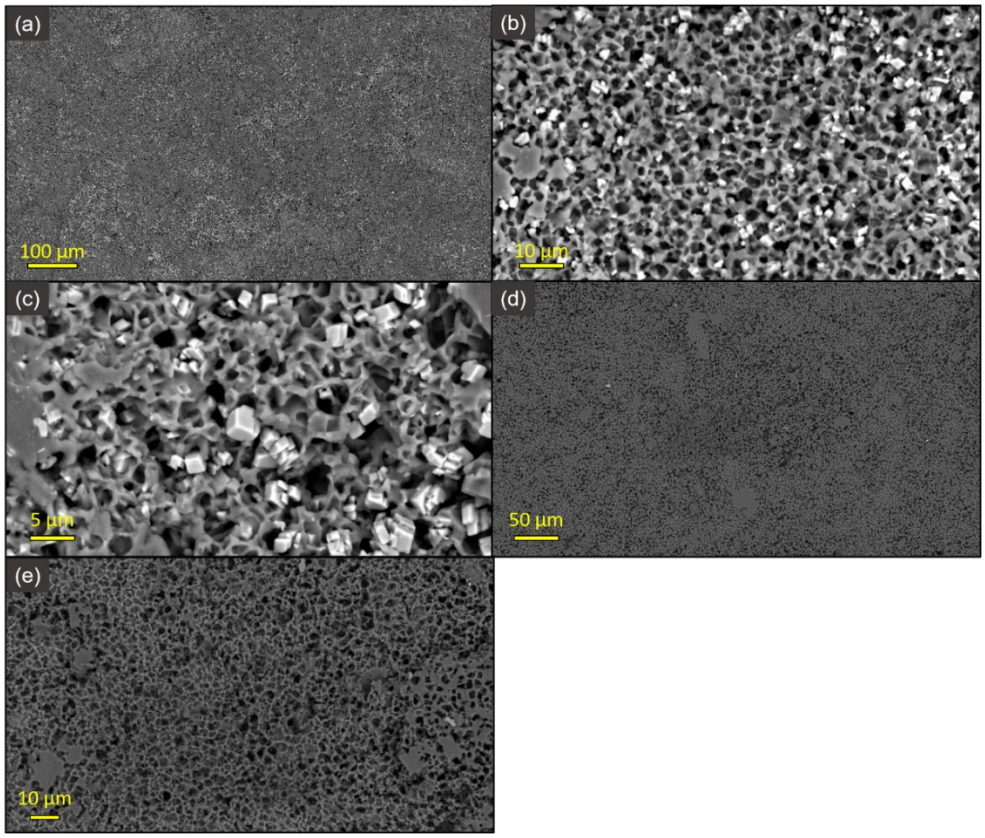

Figure S3. SEM Morphology of the FKM_2M surface prior to mild acid treatment. Following the curing-cum-stamping process, residual calcite crystals get stuck on the substrate. Figure S3(a-e) illustrate gradual dissolution of the crystals by mild acid treatment, followed by washing with DI water.

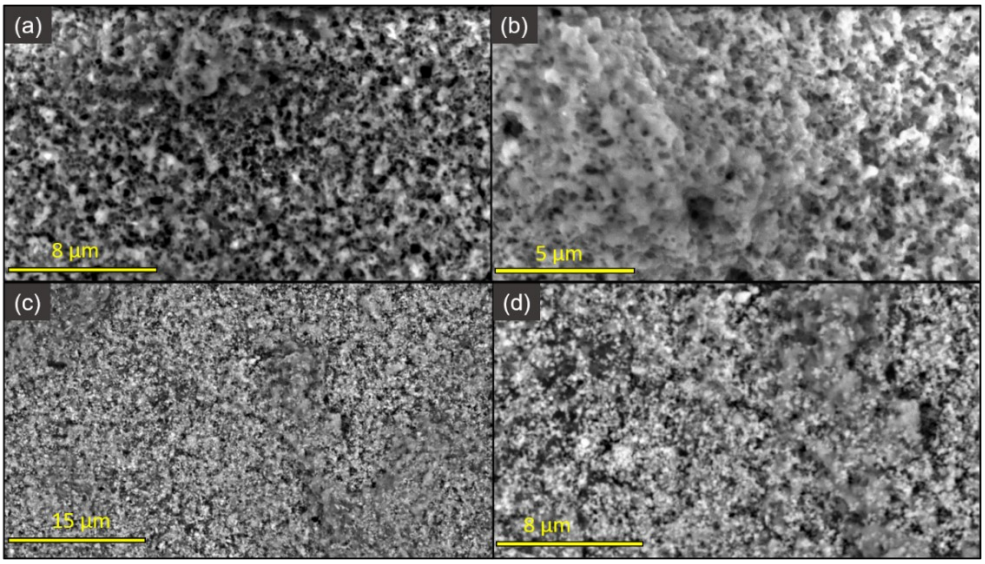

Figure S4. SEM Morphology of the FKM_0.2M surface prior to mild acid treatment. Following the curing-cum-stamping process, residual calcite crystals get stuck on the substrate. Figure S4(a-d) show morphology at various stages of dissolution of the residual calcite crystals by mild acid treatment.

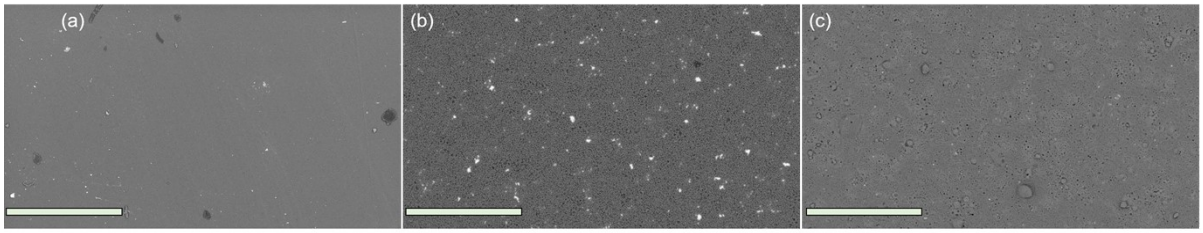

Figure S5. Low resolution SEM image of the transfer-printable molds for FKM (a), FKM_2M (b), and FKM_0.2M (c). Note that Figure (a) has no calcite crystal on the steel surface. The scale bar is 300 µm.

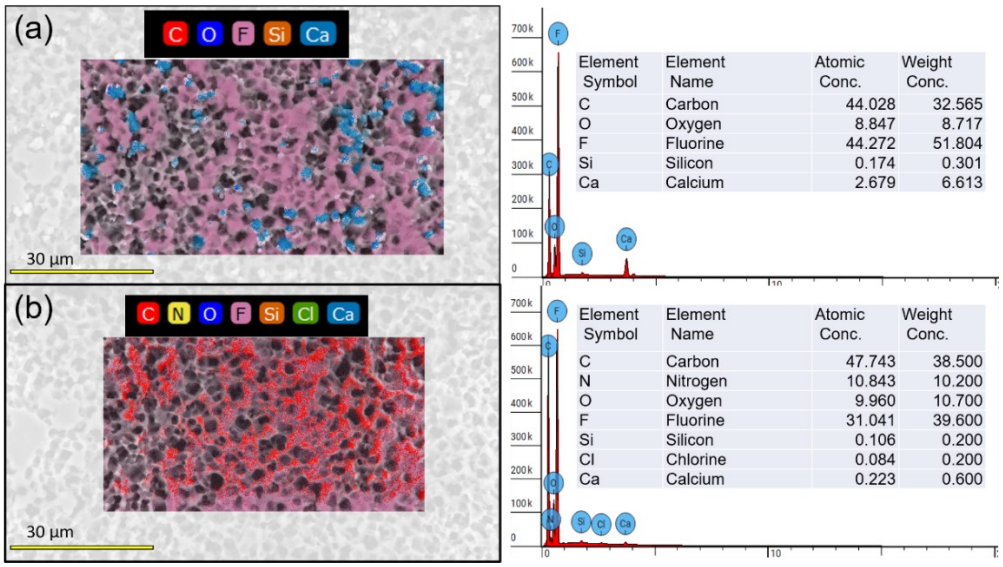

Figure S6. EDAX elemental mapping and corresponding spectra of the FKM_2M surface before (a), and after (b) dissolution of calcite crystals.

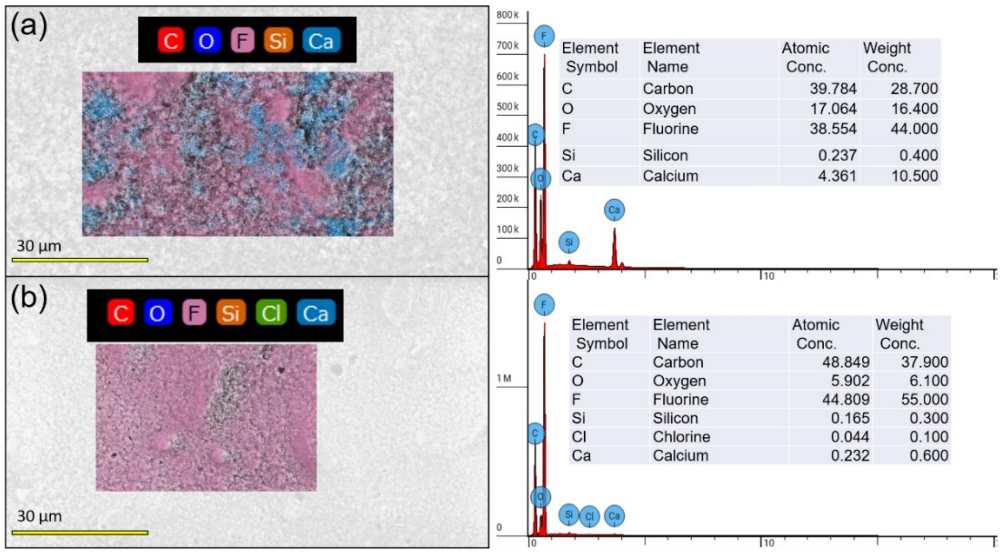

Figure S7. EDAX elemental mapping and corresponding spectra of the FKM_0.2M surface before (a), and after (b) dissolution of calcite crystals.

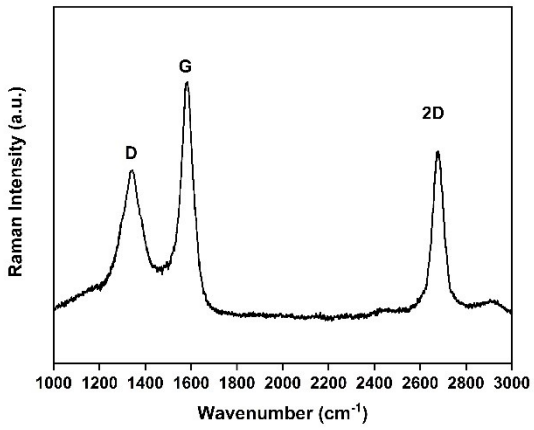

Figure S8. Raman spectra of the LIG/PI substrate. A sharp 2D peak at around 2700 cm^{-1} confirms the formation graphene.

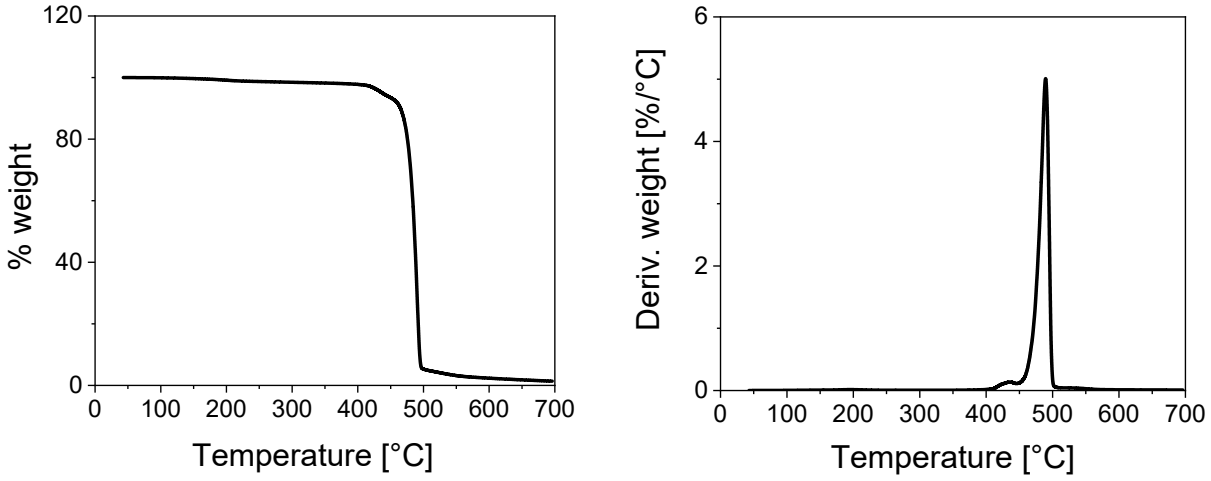

Figure S9. Thermogravimetric analysis (TGA) was performed on a thermo-balance TGA/SDTA 851 (Mettler-Toledo) with the temperature range of 30°C-700°C and heating rate of 10°C/min under nitrogen atmosphere. The plot of weight loss% as a function of temperature (left) and a derivative plot (right) illustrate exceptional thermal stability window of the FKM elastomer. The maximum degradation temperature was found to be around 488°C.

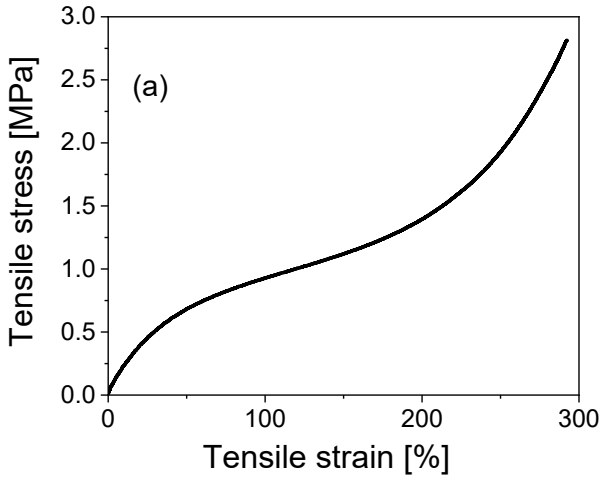

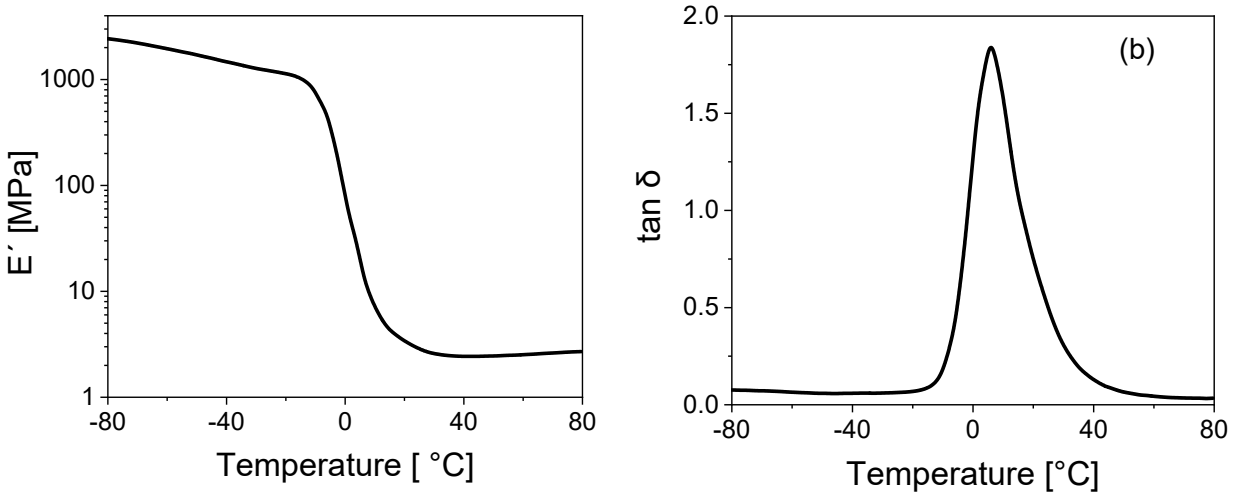

(c)

Figure S10. Mechanical characterization of the FKM elastomer. (a) Uniaxial tensile stress-strain curve plotted for cured FKM substrate. Uniaxial tensile test of the compound was carried out (DIN 53504) using dumbbell specimens (DIN S2). A universal testing machine (UTM, Zwick/Roell-Z010, equipped with 100 N force transducer, Ulm, Germany) was employed and the experiment was performed at ambient temperature with a cross-head speed of 200 mm/min. The parameters obtained from tensile measurements are tabulated in Table S3. Since it consists of only curing agents, tensile strength value corresponds mainly to crosslinking contribution. The % elongation at break could be explained in terms of the mobility of the elastomer chain. If the mobility of the polymer chain is restricted by chemical crosslinking, elongation at break (%) tends to decrease. Higher magnitude of moduli at 100% and 200% indicates higher extent of crosslinking, which is in good agreement with the $(M_H - M_L)$ value obtained from rheometric study. (b) Storage modulus (E') and (c) *tan* δ as a function of temperature, obtained from dynamic mechanical analysis. The dynamic mechanical properties of the FKM were investigated using Eplexor 2000N (Netzsch Gabo Instruments GmbH). Rectangle specimens of 35 × 10 × 2 mm^3 dimension was cut out from the sheet. The temperature range was set from

-80 to 150°C at a heating rate of 2K/min. The frequency of the test was 10 Hz under 0.5% dynamic strain and 1% static strain. Storage modulus (E′), loss modulus (E″), damping factor (tan δ) were evaluated. The storage modulus (E') value in the rubbery region (positive temperature range in Fig. S2b) indicates typical rubber-filler interaction in composite. As no filler materials were present in FKM, the E' includes mainly the crosslinking contribution. From Fig. S2c, glass transition temperature (T_g) was obtained, which was ~6°C for FKM.

Table S2. Parameters obtained from tensile stress-strain measurement

Parameters	Obtained value
Tensile strength (MPa)	2.8
Elongation at break (%)	290
100 % modulus (MPa)	0.9
200 % modulus (MPa)	1.3

Table S3. Literature survey and triboelectric output comparison of recently reported literature containing stretchable TENG.

Reference	Max. Strain	Composition of TENG	Maximum output voltage and current	Maximum power density
[1]	120%	PDMS/Crumpled Graphene	83.0 V, 25.78 μA	0.25 mW/cm^2
[2]	300%	Silicone/glass beads	370 V, 9.5 μA	-
[3]	500%	Polysiloxane/EGaIn	557–604 V, 11.8–12.9 μA cm^{-2}	(1 mW cm^{-2})
[4]	2500%	PUA + silver + liquid metal	100 V, 4 μA cm^{-2}	40 μW cm^{-2}
[5]	171%	catechol-chitosan-diatom hydrogel	110 V, 3.8 μA	29.8 mW/m^2
[6]	20%	3D printed metal-core silicone-copper (Cu)	0.38 μA, 5.75 V	31.39 mW/m^2
[7]	100%	Fermat-spiral based energy yarn/PVDF-TrFE	105 V, ≈1.2 μA	-
[8]	80%	PDMS/SWCNT	870 V, 60 μA	8 W/m^2
[9]	160%	Fluorinated ethylene propylene/TPU-Ag NW-PDMS	~250 V, ~40 μA	20 mW m^{-3}
[10]	1160%	PAAm-LiCl hydrogel/PDMS	145 V, 1.5 μA	35 mW m^{-2}
[11]	190%	Epichlorohydrin (GECO/5%CB-PDMS)	192 V, 27 μA	540 μW/cm^2
This work	290%	Micropatterned FKM/LIG electrode	148 V, 9.6 μA	715 mW/m^2

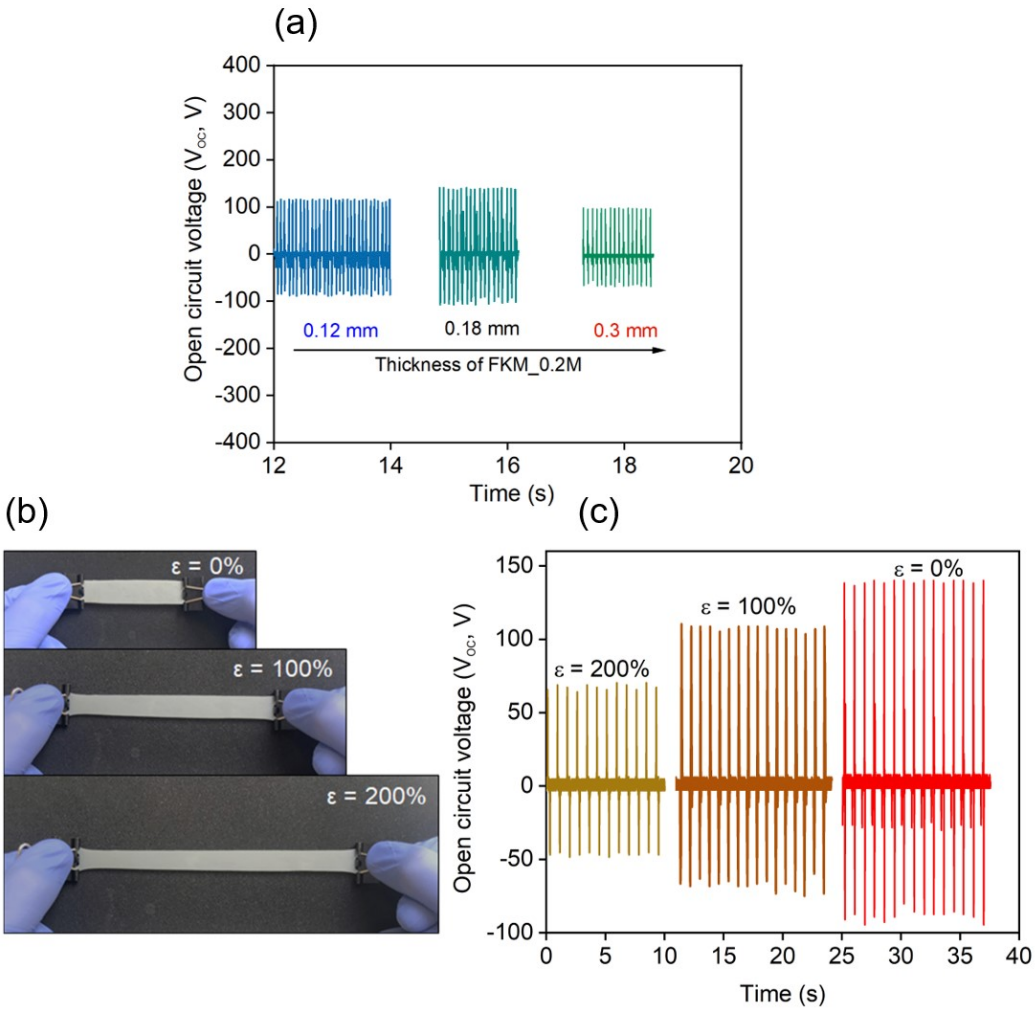

Figure S11. (a) Effect of thickness on the output characteristic of the FKM_0.2M/LIG film. The optimum thickness of the film was found to be 0.18 mm, below and beyond which, output V_{OC} drops. (b) Effect of strain% on the triboelectric output voltage of the STENG. Images of the typical FKM_0.2M/LIG film under various stages of elongation. Note that the membrane is ultrastretchable. (c) A decrease in overall output voltages with strain (ε%) of up to 200% can be explained in terms of apparent decrease in STENG thickness.

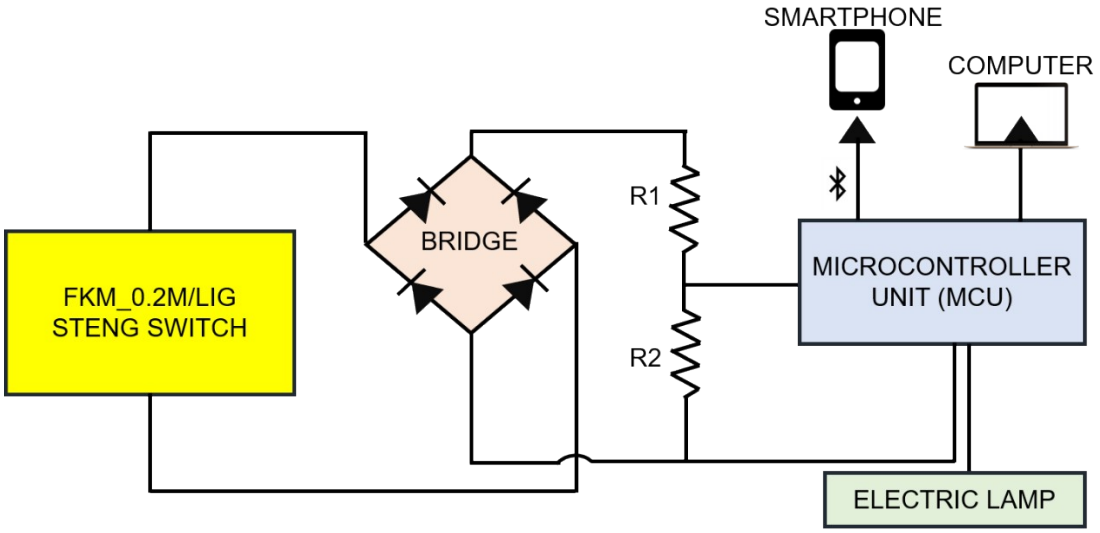

Figure S12. Electrical circuit configuration of the FKM_0.2M/LIG STENG-based electronic touch module as a smart switch for home application. In the demonstration, the FKM_0.2M/LIG STENG is attached to a bridge rectifier for AC to DC conversion, followed by two resistors (R1 and R2) and a microcontroller unit. The microcontroller is powered by 5V USB output from a computer with program terminal. In case of smartphone command, the microcontroller can be connected to any external power supply. The electric candle lamp is connected to the digital input port of the MCU. When finger touches the FKM_0.2M/LIG STENG, contact electrification produces electrical signal in terms of DC voltage that is being read by the microcontroller. The command is then transferred and executed in terms of light on/off control.

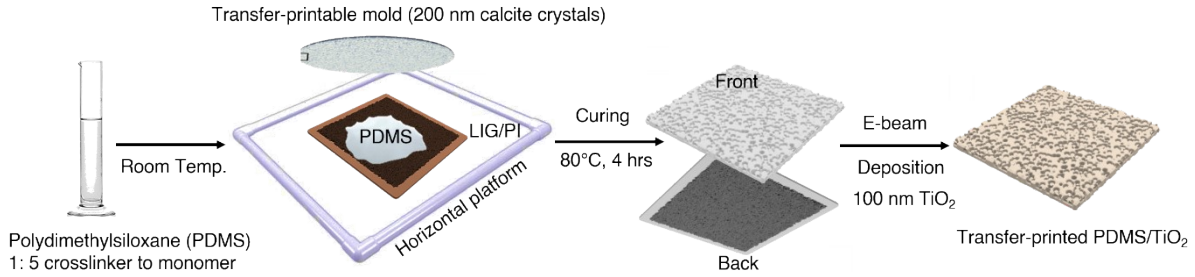

Figure S13. Schematic illustration of the micropatterned PDMS/TiO_2 fabrication.

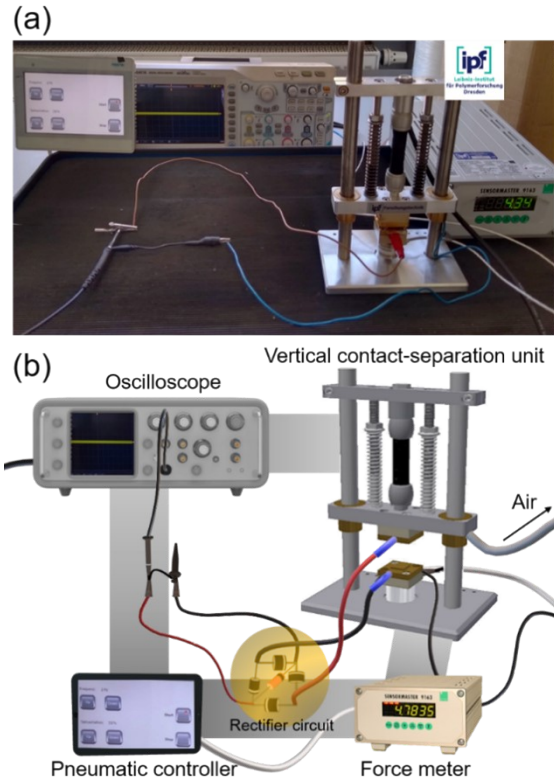

Figure S14. Detailed measurement setup for the triboelectric characterization of the STENG/TENG. For the contact-separation device, an in-house developed vertical contact-separation unit, connected to a Pneumatic actuator (Festo Corp.) was employed. Total vertical contact force generated by the pneumatic motor was 15 N/cm^2. For the voltage values, STENG/TENG were collected to a Rigol DS4024 Digital storage Oscilloscope. To measure the force, the controller was connected to a force sensor (Burster Sensormaster 9163).

Supporting Movie S1: Illumination of 20 LEDs by Triboelectric contact separation motion

Supporting Movie S2: Demonstration of Smart tribo-switch to turn on/off an electric lamp

Supporting Movie S3: Demonstration of energy harvesting by STENG in terms of running a calculator by capacitor charged by STENG.

References:

1. Chen et al., *Nano Energy,* 2019, **58**, 304–311.

2. Li et al., *Beilstein J. Nanotechnol.,* 2021,**12**, 402–412.

3. Pan et al., *Adv. Mater. Technol.,* 2020, **5**, 2000754.

4. Parida et al., *Nature Commun.,* 2019, **10**, 2158.

5. Kim et al., *Nano Energy,* 2021*,* **82**, 105705.

6. Tong et al., *Nano Energy,* 2020*,* **75**, 104973.

7. Zhang et al., *Adv. Mater.,* 2021, **33**, 2100782.

8. Matsunaga et al., *Nano energy,* 2020, **67**, 104297.

9. Ren et al., *Adv. Energy Mater.,* 2020, **10**, 2001770.

10. Pu et al., *Sci. Adv.,* 2017*,* **3**, e1700015.

11. Natarajan et al., *ACS Appl. Elect. Mater*. 2020, **2***,* 4054-4064.